Kinetics and Catalysis, Vol. 41, No. 4, 2000, pp. 572–583. Translated from Kinetika i Kataliz, Vol. 41, No. 4, 2000, pp. 628–640.

Formation of Vanadia–Titania Oxide Catalysts

G. A. Zenkovets, G. N. Kryukova, S. V. Tsybulya, E. M. Al'kaeva, T. V. Andrushkevich, O. B. Lapina, E. B. Burgina, L. S. Dovlitova, V. V. Malakhov, and G. S. Litvak

Boreskov Institute of Catalysis, Siberian Division, Russian Academy of Sciences, pr. akademika Lavrent'eva 5, Novosibirsk, 630090 Russia

Received January 27, 1999

Abstract—The formation of vanadia–titania catalysts was studied with a complex of physicochemical methods. The use of highly dispersed anatase with a defect structure results in the formation of coherent boundaries of coalescence of the V_2O_5 and TiO_2 crystallites with the ratio V : Ti =1 : 1 in a wide range of vanadium and titanium concentrations. The catalysts containing coherent boundaries are active and selective in β-picoline oxidation to nicotinic acid.

INTRODUCTION

Until now, a great number of publications have been devoted to studying vanadia–titania catalysts by modern physicochemical methods [1–13]. This is due to the high activity and selectivity of these catalysts in most partial oxidation reactions that are important for industry, for example, the oxidation of *o*-xylene to phthalic anhydride [1, 11, 14–17] and of toluene to benzaldehyde [18], the ammoxidation of alkylaromatics [19–23], the reduction of nitrogen oxides with ammonia [24–26], etc. [27, 28].

One of the most common methods for preparing the vanadia–titania catalysts is by impregnating TiO_2 with an anatase structure by solutions of vanadyl oxalate or ammonium vanadate, followed by drying and thermal treatment in the range of 350–500°C [8, 11, 17, 29, 30]. As is shown in [31, 32], vanadium–titanium catalysts that are active and selective in oxidizing of *o*-xylene to phthalic anhydride can be prepared by thermally treating a mixture of vanadia and anatase. Methods for depositing vanadium onto anatase using vanadyl chloride [29, 33–37] or vanadium organometallic compounds [29, 36, 37], as well as the ion-exchange method [38], are also known. It has been found that the active sites on which vanadium is adsorbed during the preparation of catalysts by the above methods are surface hydroxyl groups [23, 29, 33, 34, 39–41].

Special attention was paid in the literature to the study of vanadia–titania catalysts with a low vanadium content corresponding to a monolayer or near-monolayer coverage of the TiO_2 surface. According to most data, these catalysts exhibit the highest activity in the above reactions and, moreover, are the most convenient model systems for studying the interaction between vanadium and the support.

In the vanadia–titania catalysts, the formation of isolated monooxovanadyl [2–4] and dioxovanadyl [7, 31, 34, 44] groups with the tetrahedral or octahedral coordination of vanadium, which are strongly bound with the anatase surface, and V_2O_5 clusters, which are more weakly bound with the surface, [45, 46] has been found.

Note that a structural interaction between V_2O_5 and anatase in the vanadia–titania catalysts prepared by the methods published was not observed experimentally. By comparing the structures of anatase and V_2O_5, it was suggested [49, 50] that a coherent boundary formed by the planes (010) V_2O_5 and (100) TiO_2 or (100) V_2O_5 and (001) TiO_2 may exist between these oxides. The formation of a thin amorphous layer of V_2O_5 on the anatase surface was found [51] in the vanadia–titania system by electron microscopy.

The interaction between vanadia and anatase is a topical problem because this interaction is believed to change the O–O bond length in the structure of supported vanadia [50] and to increase the concentration of terminal V=O bonds at the surface that are responsible for selective oxidation [1–3, 52]. Recently, data on a significant role of the V–O–Ti bonds in selective oxidation were published [11].

In this work, we studied the formation of vanadia–titania catalysts, over a wide range of vanadium and titanium concentrations. The catalysts were prepared by mixing vanadyl oxalate and titanium dioxide (anatase). These catalysts are active and selective in oxidizing formaldehyde and β-picoline to the corresponding carboxylic acids [53–55], as well as in the ammoxidation of methylpyrazine to pyrazine amide [56].

EXPERIMENTAL

Samples were prepared from a suspension of titanium dioxide (anatase) prepared by the sulfate technology and a solution of vanadyl oxalate in a sputtering dryer, followed by drying at 110°C and thermal treatment in an air flow in the temperature range 200–700°C for 4 h. The total amount of vanadium and titanium in

0023-1584/00/4104-0572$25.00 © 2000 MAIK "Nauka/Interperiodica"

the catalysts was determined by atomic-absorption spectrometry on a Saturn spectrometer.

X-ray diffraction experiments were carried out on a URD-63 diffractometer with a graphite monochromator using CuK_α radiation. The X-ray diffraction patterns were recorded by point-by-point scanning with a 0.02° step in the 2θ range and 20 s accumulation time per point.

The lattice parameters of anatase were refined by the least-squares method using a special program [57], taking into account 3–7 lines, depending on the resolution of the diffraction peaks in the angle region 50–70°.

The microdistortions of the titanium dioxide structure and the size of the regions of coherent scattering (RCS) were estimated by the Cauchy approximation method [58] using the (101) and (200) diffraction peaks. The amount of the rutile phase was determined according to [59].

An electron-microscopic study was performed on a JEM-4000 FX instrument with a resolution of 0.14 nm and an accelerating voltage of 400 kV. The elemental composition of samples was studied on a Philips CM-200 transmission electron microscope with an EDAX DX-4 thin-film microanalysis system supplied with an X-ray energy-dispersion detector (the detection sensitivity is 0.1 wt %).

IR spectra were recorded on a BOMEN MB-102 spectrometer. Samples were prepared as pellets with CsI and suspensions in a fluorinated oil. In the second case, the samples were cooled after calcination to room temperature without contact with air and then the suspension was prepared in a special box. This allowed us to exclude water from both the CsI matrix and adsorption on the surface of samples.

The ^{51}V NMR spectra were recorded on a Bruker MSL-400 spectrometer at a frequency of 105.2 MHz, a radio-frequency pulse duration of 5 μs, and a pulse repetition frequency of 1–10 Hz. The ^{51}V NMR MAS spectra (magic angle sample spinning) were measured on an NMR Rotor Consult ApS instrument at a rate ranging from 4 to 15 kHz. The chemical shifts were measured relative to $VOCl_3$ as an external standard. The MAS spectra parameters and the constant of quadrupole coupling (C_Q) were calculated according to a procedure [60].

Thermal analysis was carried out on a DQ 1500-D instrument at temperatures up to 1000°C; the sample heating rate was 10 K/min.

Chemical phase analysis by selective dissolution was performed according to a procedure described in [61, 62]. The dynamic regime of dissolution consisted in continuous changes in the solvent composition from H_2O to 1.2 M HNO_3 and in the temperature from 20 to 60°C at the first stage and in going to an HF solution (1 : 5) and increasing the temperature up to 70–80°C at the second stage.

The catalytic properties of the vanadia–titania catalysts in β-picoline oxidation to nicotinic acid were studied in a differential reactor of a flow-circular setup with a 0.25–0.5 mm fraction of the catalyst at 250°C and the following concentrations of the starting components (vol %): β-picoline, 1; oxygen, 20; water vapor, 30; nitrogen, the rest. The reaction mixture components were analyzed by chromatography. The β-picoline conversion rates and selectivities with respect to the reaction products (nicotinic acid, β-pyridinecarbaldehyde, and CO_2) as functions of β-picoline conversion were measured for each sample. The catalytic properties were compared at a conversion of 50%.

RESULTS

Crystal structure as studied by XRD analysis. It follows from Table 1 that individual titanium dioxide is anatase at a temperature of 110–700°C. After calcination of vanadyl oxalate at a temperature of 300°C or higher, the well crystallized V_2O_5 phase is observed. Only the anatase phase is detected at 110°C in the binary vanadium–titanium samples containing less than 30 wt % V_2O_5, and anatase and vanadyl oxalate are found at higher concentrations. The phase composition of calcined samples depends heavily on the vanadium content and calcination temperature. The samples with a low vanadium content (3–5 wt % V_2O_5 and 97–95 wt % TiO_2) contain only anatase at temperatures of up to 650°C, and at a temperature of 700°C, rutile also appears. With an increase in vanadium content, the V_2O_5 phase is detected, along with anatase in the temperature range 300–600°C. The temperature of the V_2O_5 formation decreases with an increase in the vanadium content. Moreover, in the samples containing at least 30 wt % V_2O_5, rutile, along with anatase and V_2O_5, forms at 300°C, and its amount increases with an increase in the calcination temperature, for example, in a sample with 50 wt % V_2O_5 and 50 wt % TiO_2 as follows.

T, °C	300	400	450	500	600	700
Amount of rutile, wt %	10	15	25	40	90	100

After calcination at 700°C, rutile and V_2O_5 are detected in these samples.

As seen in Table 2, an increase in the calcination temperature for titanium dioxide and the binary samples results in a significant increase in the lattice parameter c of anatase, whereas the lattice parameter a varies slightly. At low calcination temperatures (300–400°C), microdistortions of the anatase crystal lattice are observed in binary samples, as well as in pure titanium dioxide, but these microdistortions are less pronounced in the binary samples (at the corresponding temperature) than in pure TiO_2. It follows from Table 2 that microdistortions in the binary catalysts disappear

Table 1. Effect of the calcination temperature and chemical composition of the vanadium–titanium samples on the phase composition

Chemical composition, wt %	110°C	300°C	400°C	450°C	500°C	550°C	600°C	700°C
100% TiO_2	anatase	anatase	anatase	anatase	anatase	anatase	anatase	anatase
3% V_2O_5, 97% TiO_2	anatase	anatase	anatase	anatase	anatase	anatase	anatase	rutile anatase
5% V_2O_5, 95% TiO_2	anatase	anatase	anatase	anatase	anatase	anatase	anatase	rutile anatase
10% V_2O_5, 90% TiO_2	anatase	anatase	anatase	anatase	anatase	anatase, V_2O_5,	anatase, V_2O_5,	rutile, V_2O_5
15% V_2O_5, 85% TiO_2	anatase	anatase	anatase	anatase	anatase, V_2O_5,	anatase, V_2O_5,	anatase, V_2O_5,	rutile, V_2O_5
20% V_2O_5, 80% TiO_2	anatase	anatase	anatase	anatase, V_2O_5	anatase, V_2O_5,	anatase, V_2O_5,	anatase, V_2O_5,	rutile, V_2O_5
30% V_2O_5, 70% TiO_2	anatase, $VOC_2O_4 \cdot nH_2O$	anatase, V_2O_5, rutile	anatase, V_2O_5, rutile	anatase, V_2O_5, rutile	anatase, V_2O_5, rutile	anatase, V_2O_5, rutile	rutile, V_2O_5, anatase	rutile, V_2O_5
50% V_2O_5, 50% TiO_2	anatase, $VOC_2O_4 \cdot nH_2O$	anatase, V_2O_5, rutile	anatase, V_2O_5, rutile	anatase, V_2O_5, rutile	anatase, V_2O_5, rutile	anatase, V_2O_5, rutile	rutile, V_2O_5, anatase traces	rutile, V_2O_5
75% V_2O_5, 25% TiO_2	anatase, $VOC_2O_4 \cdot nH_2O$	anatase, V_2O_5, rutile	anatase, V_2O_5, rutile	anatase, V_2O_5, rutile	anatase, V_2O_5, rutile	anatase, V_2O_5, rutile	rutile, V_2O_5, anatase traces	rutile, V_2O_5
100% V_2O_5	$VOC_2O_4 \cdot nH_2O$	V_2O_5	V_2O_5	V_2O_5	V_2O_5	V_2O_5	V_2O_5	V_2O_5

more rapidly with an increase in the temperature than in TiO_2.

Thermal analysis. The thermal analysis data for the starting titanium and vanadium compounds and binary samples (Fig. 1) indicate that two endo effects are detected for TiO_2 at 170 and 615°C, which are accompanied by a weight decrease. According to [63], the endo effects are due to dehydration and the removal of sulfate ions.

When vanadyl oxalate is thermally treated, the following effects are observed: endo effects at 200 and 350°C with a weight decrease, exo effects at 220 and 325°C, also with a weight decrease, and an exo effect at 370°C with a weight increase, which are typical of vanadyl oxalate decomposition and the formation of V_2O_5.

The thermal analysis curves for the binary samples indicate a change in the nature of thermal decomposition as compared to pure TiO_2 and vanadyl oxalate. Only the first endo effect, which is typical of the vanadyl oxalate decomposition but shifted to a low-temperature region and accompanied by substantial weight loss, is clearly pronounced for the samples containing less than 30 wt % V_2O_5. A small exo effect at 220°C is also observed. In increasing the vanadium content, the shape of the weight loss curve changes and the temperature of the second endo effect decreases.

Table 2. Effect of the chemical composition and calcination temperature of titanium dioxide and vanadium–titanium samples on the lattice parameters of anatase and on the microdistortion value ε

Chemical composition, wt %	*T*, °C	*a*, Å	*c*, Å	ε
TiO_2	300	3.793(3)	9.41(2)	0.0015
	400	3.790(1)	9.42(1)	0.0026
	500	3.789(1)	9.511(2)	0.0025
	650	3.7871(3)	9.516(1)	0.0001
5% V_2O_5, 95% TiO_2	400	3.791(1)	9.41(1)	0.0013
10% V_2O_5, 90% TiO_2	400	3.791(3)	9.40(1)	0.0019
20% V_2O_5, 80% TiO_2	300	3.789(1)	9.37(2)	0.0014
	400	3.790(1)	9.38(2)	0.0010
	500	3.788(1)	9.515(4)	0.0004

V_2O_5, wt %	0	5	10	15	20	50
T, °C	615	590	565	540	515	505

In addition, endothermic effects appear at 650 and 715°C, which are typical of the V_2O_5 melting and the formation of a solid solution of vanadium in rutile [64, 65]. With an increase in the vanadium content of the samples containing at least 30 wt % V_2O_5, the thermal effects typical of vanadyl oxalate decomposition and the endo effects at 500 and 670°C with weight loss are observed. The latter endo effect is due to the melting of vanadium pentoxide.

Electron-microscopic study of samples. The microstructure of the starting titanium dioxide consists of 70–90 nm aggregates, which are highly dispersed, strongly disordered, and loosely packed 3–8 nm crystallites of anatase.

The formation of highly dispersed (~1 nm) vanadia located at the surface and between the crystallites of highly dispersed anatase is observed in the micrographs of samples that contain less than 30 wt % V_2O_5 and calcined at a temperature above 300°C but lower than the temperature of the beginning of the second endo effect on the DTA curves (Fig. 2).

After the calcination of these samples at the temperature of the beginning of the second endo effect, their microstructure changes dramatically. The electron micrographs show that large anatase crystals measuring ~70 nm are joined along specific crystallographic directions with the crystallites of vanadium pentoxide to form a pronounced coherent boundary between them. As can be seen in micrographs (Fig. 2), the coherent boundary between vanadia and titania forms in different ways depending on the vanadium concentration. In the samples with a low vanadium content (5 wt % V_2O_5), comparatively small vanadia crystallites (~1.5 nm) coalesce with regularly structured anatase crystallites. It is seen that the formation of this boundary results in some disordering of the anatase crystallite at the site of its junction with the vanadia crystallite, whereas the structure of the rest of the TiO_2 crystal remains regular.

Coarse anatase crystallites of 70–90 nm size joined with the vanadia crystallites along specific crystallographic directions are seen on the electron micrographs of the samples containing 10–20 wt % V_2O_5 and 90–80 wt % TiO_2, and a regular coalescence boundary between them is clearly seen.

The formation of the structure of coherent coalescence between the crystallites of vanadia and titania is observed in Fig. 2d for the sample with a higher vanadium content (50 wt % V_2O_5–50 wt % TiO_2). Here the blocks of the TiO_2 and V_2O_5 phases alternate with each other inside an isolated particle of about 70–90 nm in size across its entire volume.

It follows from the results that a tendency to the formation of contact regions between the TiO_2 and V_2O_5 particles starting from single regular boundaries to the development of structures of coherent coalescence is observed with an increase in the vanadium concentration in the catalysts.

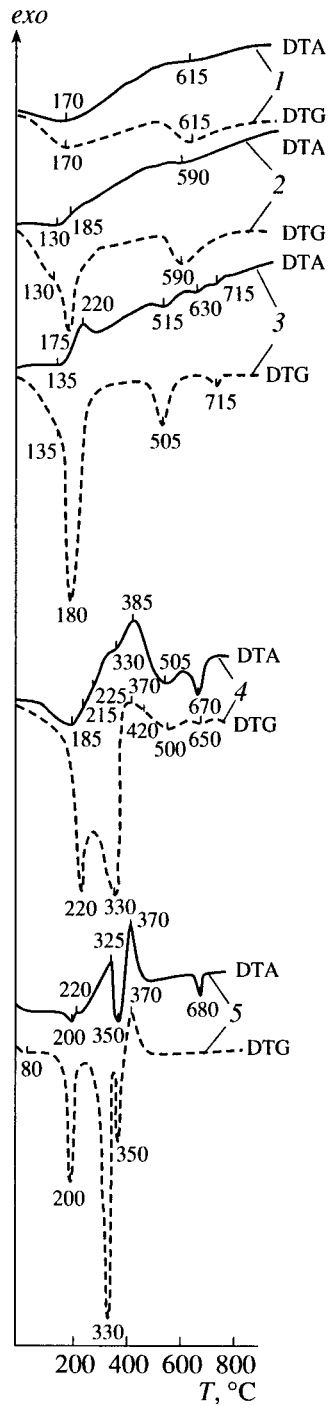

Fig. 1. DTA and DTG curves for (*1*) starting TiO_2, (*2*) 5 wt % V_2O_5–95 wt % TiO_2, (*3*) 20 wt % V_2O_5–80 wt % TiO_2, (*4*) 50 wt % TiO_2–50 wt % V_2O_5, and (*5*) starting vanadyl oxalate.

The observed coherent boundaries and the structures of coherent coalescence are reasonably stable. They are retained under the action of an electron beam and during thermal treatment in an oxidative atmosphere up to the melting point of V_2O_5.

Figure 3 presents the X-ray spectrum of the sample containing 20 wt % V_2O_5–80 wt % TiO_2 recorded directly in the region of the coherent boundary of coa-

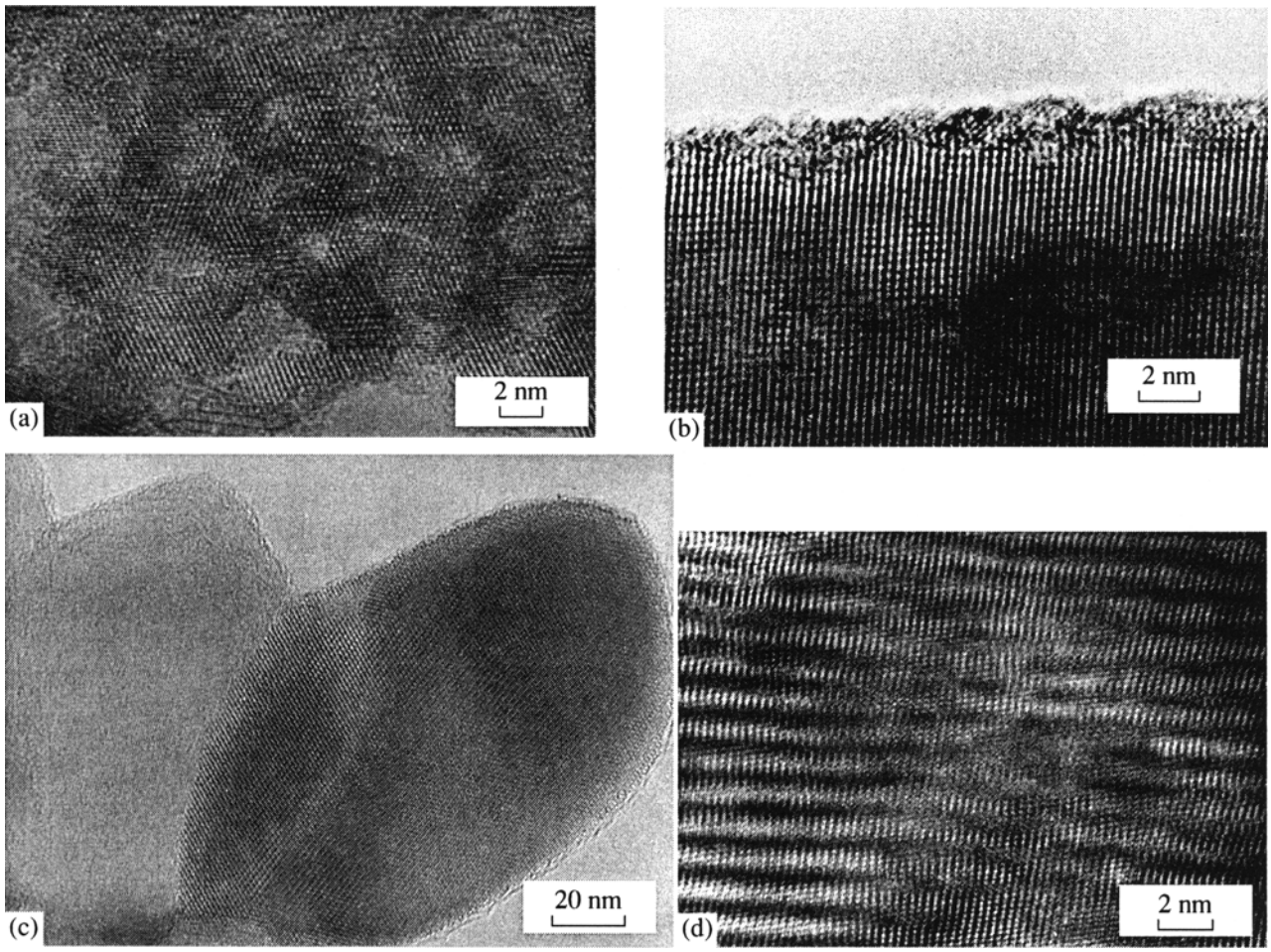

Fig. 2. Electron micrographs of samples: (a) 20 wt % V_2O_5–80 wt % TiO_2 calcined at 400°C, (b) 5 wt % V_2O_5–95 wt % TiO_2 calcined at 590°C, (c) 20 wt % V_2O_5–80 wt % TiO_2 calcined at 500°C, and (d) 50 wt % V_2O_5–50 wt % TiO_2 calcined at 500°C.

lescence formed by the vanadia and titania crystallites. It is seen that the V : Ti ratio is close to 1. According to microanalysis data, the vanadium concentration in the region of the coalescence boundary is 51.8 at % and the titanium concentration is 48.2 at %; at the same time, vanadium is not found in the region of the TiO_2 crystal that is far from the boundary.

IR-spectroscopic study of samples. The IR spectra of the binary samples containing less than 30 wt % V_2O_5 and calcined at lower than 650°C, as well as the spectra of pure titanium dioxide, correspond to that of anatase (Fig. 4). The spectra of the binary samples dried and calcined at temperatures lower than that of the beginning of the second endo effect in the thermal analysis curves, as well as for the starting TiO_2 in the range 1200–970 cm^{-1}, exhibit absorption bands indicating the presence of sulfate ions in the anatase structure with a symmetry lower than C_{2v} [66, 67]. In the regions of 2700–3600 cm^{-1} and 1650 cm^{-1}, the absorption bands attributed to hydroxyl groups and water molecules bound by strong hydrogen bonds [68] are seen (they are observed in the spectra taken in both the CsI matrix and the fluorinated oil) (Fig. 5).

A comparison of the spectra of the starting titanium dioxide and binary samples calcined at the same temperature shows that, in the case of binary samples, the shape of the broad absorption band in the range of Ti–O vibrations (400–900 cm^{-1}) changes, and the absorption band in the range 900–950 cm^{-1} corresponding to the stretching vibrations of the M–O–M fragment [69, 70] becomes more intense (Fig. 6).

After calculation of the samples at a temperature above that of the beginning of the second *endo* effect in the DTA curves, the IR spectra change: the absorption bands attributed to the stretching vibrations of a sulfate group disappear; the intensities of the absorption bands in the regions 2700–3600 cm^{-1} and 1650 cm^{-1} due to hydroxyl groups and water molecules decrease significantly when the spectra are recorded in the CsI matrix, whereas the latter bands are not observed when the recording is carried out in fluorinated oil (Fig. 5). The absorption band at 1023 cm^{-1} due to the formation of the V=O fragment [69, 70] appears in the spectra of all

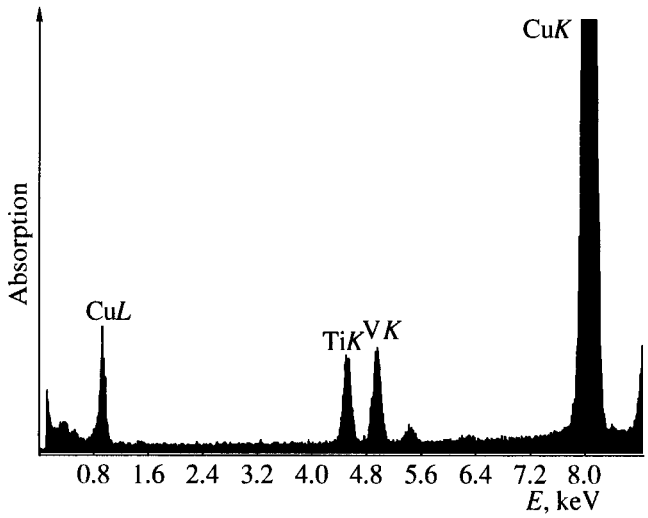

Fig. 3. X-ray spectrum of the 20 wt % V_2O_5–80 wt % TiO_2 sample calcined at 500°C in the region of the structure of coherent coalescence.

samples. The absorption band in the range of 900–950 cm^{-1} is retained, but its intensity decreases. The shape of a broad band at 400–900 cm^{-1} changes, and the absorption band at ~330 cm^{-1} shifts to the region 342–350 cm^{-1}; this can be caused by the equalization of the Ti–O bond lengths in the TiO_6 octahedra and their ordering in the anatase structure. The temperature at which the anatase structure is ordered depends on the vanadium content and significantly decreases with its increase (Fig. 4).

^{51}V NMR study of samples. The ^{51}V NMR spectra of the vanadia–titania samples are presented in Fig. 7. As can be seen, the character of the spectra depends on the vanadium content and calcination temperature. A broad anisotropic line with a maximum at –400 to –500 ppm, which corresponds to V^{5+} ions in the distorted octahedral coordination [45], is seen in the spectrum of the sample containing 3 wt % V_2O_5 and 97 wt % TiO_2 up to 750°C. With an increase in the V_2O_5 content up to 5 wt %, the spectrum with the above parameters is also observed at temperatures below 590°C. At 590°C, the ^{51}V NMR spectrum is a superposition of lines characterized by an axial anisotropy of the chemical shift with the $\sigma = 310$ ppm and $\sigma_{||} = 1270$ ppm parameters typical of V_2O_5 [45] and the line with a maximum at $\delta = -400$ to –500 ppm. When the temperature is increased to 620°C, only the spectrum typical of well-crystallized V_2O_5 is observed.

As can be seen in Fig. 7, an increase in the vanadium concentration does not result in a change in the nature of the ^{51}V NMR spectra. When the vanadium content is increased, the spectrum typical of V_2O_5 only appears at a lower temperature.

To estimate the parameters of the magnetic screening tensor and the quadrupole coupling for the anisotropic line with a maximum in the region of –400 to –500 ppm, the static spectra and MAS spectra (rotation frequency was varied from 8 to 15 kHz) for the sample with

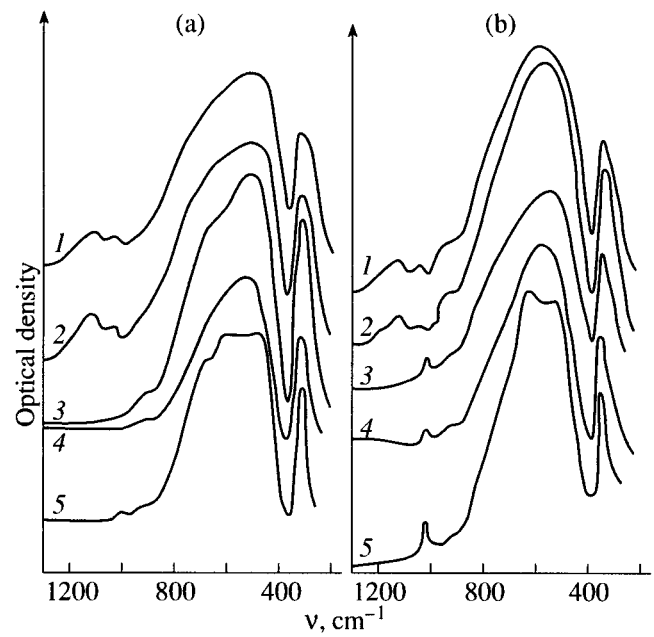

Fig. 4. IR spectra of samples: (a) 10 wt % V_2O_5–90 wt % TiO_2 calcined at (*1*) 350, (*2*) 400, (*3*) 530, (*4*) 550, and (*5*) 600°C; (b) 20 wt % V_2O_5–80 wt % TiO_2 calcined at (*1*) 300, (*2*) 400, (*3*) 450, (*4*) 500, and (*5*) 600°C. Samples were pressed as pellets with CsI.

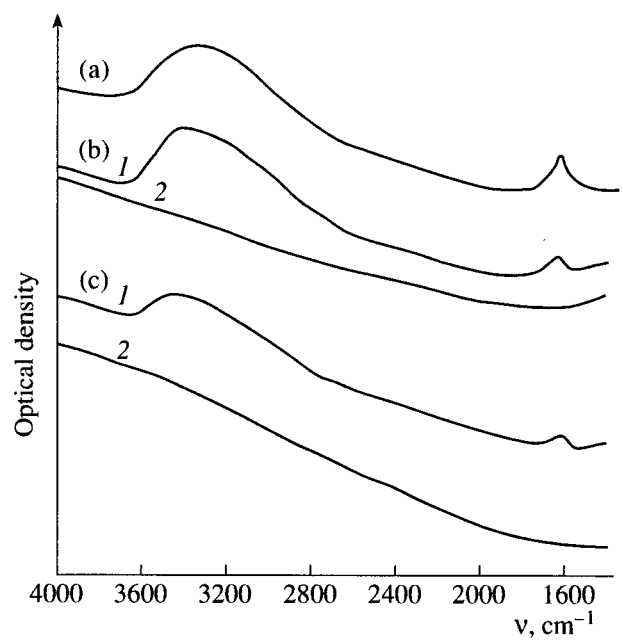

Fig. 5. IR spectra of samples: (a) TiO_2 calcined at 500°C; (b) 10 wt % V_2O_5–90 wt % TiO_2 calcined at (*1*) 300 and (*2*) 550°C; and (c) 20 wt % V_2O_5–80 wt % TiO_2 calcined at (*1*) 300 and (*2*) 500°C. Samples were used as suspensions in fluorinated oil.

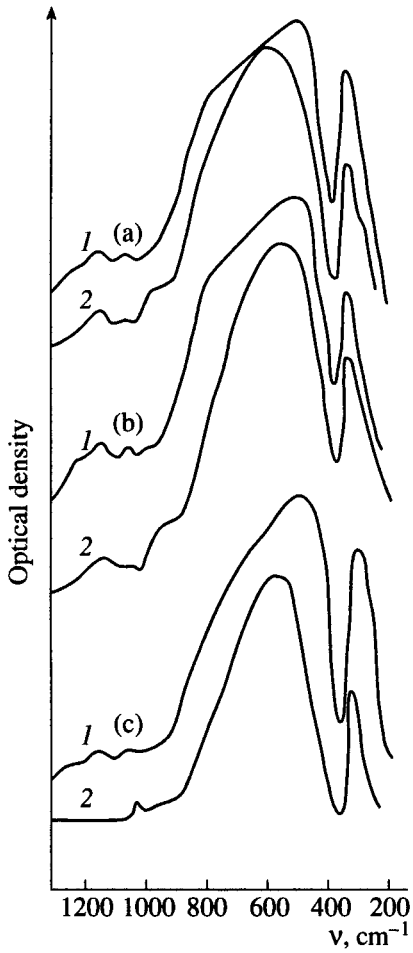

Fig. 6. IR spectra of samples: (*1*) TiO_2 and (*2*) 20 wt % V_2O_5–80 wt % TiO_2 calcined at (a) 300, (b) 400, and (c) 500°C.

20 wt % V_2O_5–80 wt % TiO_2 calcined at various temperatures (excess V_2O_5 was preliminarily washed off) were compared. Figure 8 shows that the MAS spectrum for the sample calcined at 400°C contains well-resolved side bands from pentavalent vanadium ions of two types (with prevailing I type) in the distorted octahedral coordination, which is close to V_2O_5 in anisotropy of the chemical shift but is characterized by a significantly higher quadrupole coupling constant (C_Q) (Table 3). At 450°C, the spectrum is also a superposition of these two lines, but the relative intensity of the line corresponding to V^{5+} ions of the II type decreases, indicating a decrease in the concentration of these ions in the sample. After calcination at 500°C, only one line (type III) is seen with the parameters typical of V^{5+} ions in the distorted octahedtral coordination but with a higher quadrupole coupling constant. A high quadrupole coupling constant points to a great gradient of the electrical field near the vanadium nucleus and can be a result of the formation of the V–O–Ti bonds, which substantially differ from the V–O–V bonds in V_2O_5.

A study of samples by selective dissolution. The method of selective dissolution often allows the determination of the fragmentary formulas of phases in the samples synthesized. Figure 9 presents the differential kinetic curves of dissolution of vanadium and titanium for the 20 wt % V_2O_5–80 wt % TiO_2 sample calcined at 500°C. These curves are presented in a parametric form relative to the extent of vanadium dissolution. The curves are typical of the test samples. Two vanadium species are clearly distinguishable: a species that readily dissolves as a pure compound (V_I) and a species that poorly dissolves simultaneously with titanium (V_{II}). A section of the stoichiogram corresponding to the V_{II} species (curve *3*) retains the nearly constant V : Ti molar ratios, and this fact can give evidence of vanadium and titanium entering into the composition of a compound.

Table 4 shows the V_{II} : Ti molar ratios determined from stoichiograms and the amounts of vanadium as the V_{II} species for the samples calcined at various temperatures. As can be seen, this ratio is small for dried samples. During the calcination at temperatures higher than 300°C, the V_{II} : Ti ratio and the amount of vanadium as the V_{II} species increase significantly and remain constant in a wide temperature range. With an increase in the total vanadium content, the V_{II} : Ti ratio also increases, indicating an increase in the vanadium content of the vanadium–titanium compound.

According to the electron-microscopic data, after vanadium dissolution in the form of V_I, the samples are uniform highly dispersed crystallites of anatase with a more or less homogeneous distribution of vanadium.

Some decrease in the V^{II} : Ti molar ratio is observed in the samples calcined at 500–600°C. According to electron-microscopic and microanalysis data, a size of the primary anatase crystallites is ~70 nm, and the vanadium distribution in them is nonuniform across the crystal bulk: the regions with the ratio V : Ti = 1 : 1 (coherent boundaries of coalescence between the vanadia and titania crystallites) occur, along with the regions that contain no vanadium. However, the

Table 3. ^{51}V NMR MAS spectra of the 20% V_2O_5–80% TiO_2 sample at various calcination temperatures

Chemical composition	*T*, °C	σ_1, ppm	σ_2, ppm	σ_3, ppm	C_Q, MHz	State of V^{5+} ions
20% V_2O_5–80% TiO_2	400	280	290	1260	11.5	I type
	500	170	410	1260	14.7	III type
V_2O_5	500	250	340	1230	0.8	–

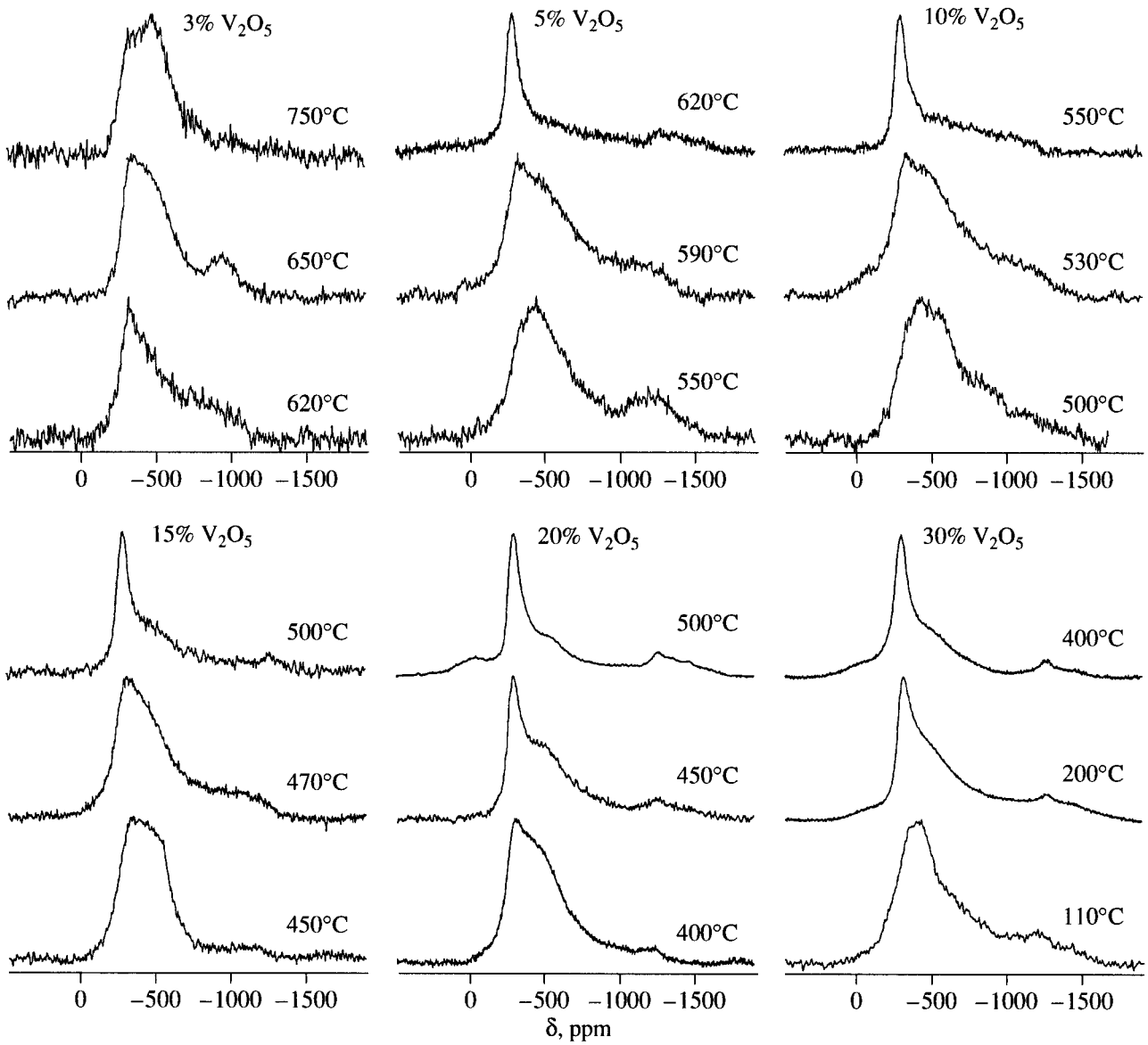

Fig. 7. ^{51}V NMR spectra of vanadium–titanium samples calcined at various temperatures.

method of selective dissolution failed to separate them. Taking into account the overall V^{II} : Ti ratio determined by selective dissolution and that obtained by microanalysis, we can calculate the weight fraction of the catalyst with the ratio V : Ti = 1 : 1 (Table 4). It is seen in Table 4 that, with an increase in the total vanadium content of the samples, the weight fraction of the regions with the ratio V : Ti = 1 : 1 increases.

Catalytic properties in β-picoline oxidation to nicotinic acid. Table 5 presents the catalytic properties of the vanadia–titania catalysts with different vanadium-to-titanium ratios calcined at the temperatures at which the coherent boundary or the structure of coherent coalescence forms. The maximum levels of activity and selectivity with respect to nicotinic acid are achieved over these catalysts independently of the component ratio. These catalytic properties are also retained at higher temperatures when the coherent boundaries or the structures of coherent coalescence are observed. The samples calcined at temperatures lower than those of the formation of these structures are less active and selective with respect to nicotinic acid.

DISCUSSION

Thus, it follows from our results that dried samples are mixtures of amorphous vanadyl oxalate and anatase that consist of highly dispersed (3–8 nm) crystallites combined into coarse aggregates. A study of the pore structure of the starting titanium dioxide [71] has shown that anatase particles are loosely packed in the aggregates, and as a result, vanadyl oxalate both pene-

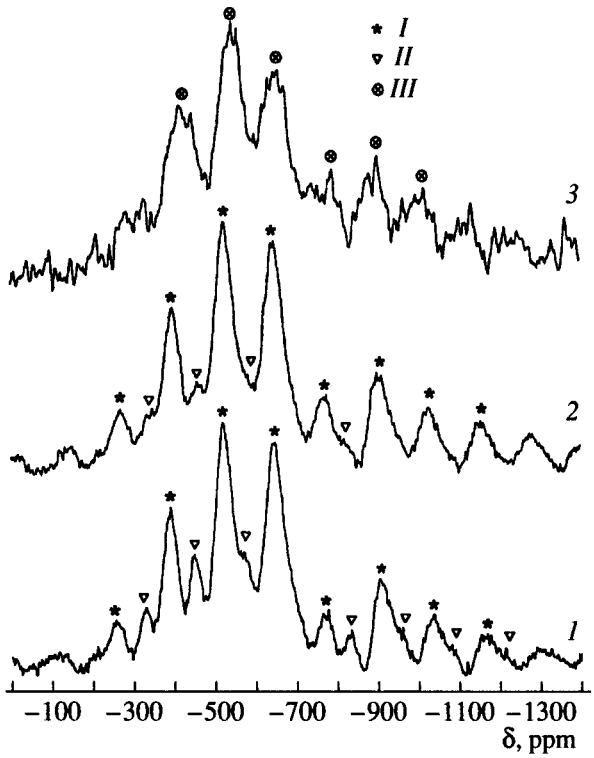

Fig. 8. ^{51}V NMR MAS spectra of 20 wt % V_2O_5–80 wt % TiO_2 samples calcined at (*1*) 400, (*2*) 450, and (*3*) 500°C and washed to remove vanadium: (*I*) side bands of the I type spectrum, (*II*) side bands of the II type spectrum, and (*III*) side bands of the III type spectrum. The rotation frequency was 12–14 kHz.

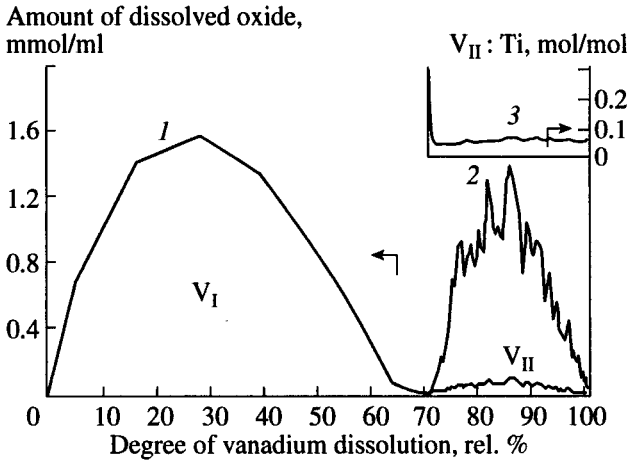

Fig. 9. Parametric kinetic curves of dissolution of (*1*) vanadium and (*2*) titanium and (*3*) the stoichiogram of a V_{II} : Ti sample of the composition 20 wt % V_2O_5–80 wt % TiO_2 calcined at 500°C.

trates inside the aggregates and occurs at their surface during drying.

As shown by ESR spectroscopy [72], only surface oxalate complexes of $(V{=}O)^{2+}$ were detected in the dried samples. The selective dissolution data (Table 4) indicate that the V_{II} : Ti molar ratio in the dried samples is close to zero, likely indicating that almost all vanadium occurs in a state not bound with titanium.

Noteworthy, a comparison between the phase composition of binary samples calcined at 300°C shows that a vanadium pentioxide phase is observed only at 30 wt % V_2O_5 content. A small amount of TiO_2 (rutile) is also detected in these samples. At the same time, when pure vanadyl oxalate is calcined at 300°C, well-crystallized V_2O_5 forms. The data of X-ray diffraction analysis agree with the above data of NMR and IR spectroscopes. In addition, the absence of a complete set of thermal effects, which are typical of the decomposition of vanadyl oxalate and formation of the vanadium pentoxide phase, from the thermoanalytical curves of the samples containing less than 30 wt % V_2O_5 suggests that a fraction of vanadium enters the structure of aggregates of titanium dioxide particles during thermal treatment and does not form the vanadium pentoxide phase. The V_2O_5 phase is formed from excess vanadyl oxalate that corresponds to the V_2O_5 content > 30 wt %. Taking into account a high specific surface area of the starting TiO_2 [71, 73] and the data [69, 74] on the vanadium content corresponding to a monolayer coverage, we can assume that at 25–30 wt % V_2O_5 the coverage of the TiO_2 surface by vanadia is close to the calculated monolayer coverage.

It is likely that a reductive medium due to CO formed upon the decomposition of a great amount of vanadyl oxalate (in samples with high vanadium contents) [75] favors the anatase–rutile phase transition, which, as is known [76], is facilitated under reductive conditions. This likely explains the appearance of a rutile phase upon the low-temperature calcination of these samples.

Thermal treatment of vanadyl oxalate located in the aggregates of highly dispersed TiO_2 particles at 300°C results in the formation of disordered crystallites of vanadia. The data of X-ray diffraction analysis and ^{51}V NMR and IR spectroscopes give unambiguous evidence for the absence of the V_2O_5 phase from the samples with the V_2O_5 content less than 30 wt %. This cannot be undecomposed vanadyl oxalate because it is not detected by ESR (only traces of the isolated surface oxalate complexes are observed [72]). As the intensity of the absorption band at 800–970 cm^{-1} in the IR spectrum, corresponding to stretching vibrations of the M–O–M bond, increases, we can assume that the V–O–V bond, which is also typical of polyvanadates, forms in these samples. The formation of polyvanadate on the surface of titanium dioxide has been found earlier [4, 47]. According to [47], its structure corresponds to decavanadate, regardless of the preparation procedure. However, the ^{51}V NMR spectrum of decavanadate [77] differs from the spectra observed by us.

The data of selective dissolution (Table 4), which demonstrate the formation of a vanadium–titanium compound with the reasonably high V : the Ti molar

Table 4. Selective dissolution data for vanadium–titanium samples calcined at various temperatures

Chemical composition, wt %	T, °C	V_{II}/Ti, mol/mol	V_{II}/V_{total}, wt %	[V : Ti = 1 : 1]*, wt %
10% V_2O_5–90% TiO_2	110	0.001	1.5	–
	300	0.051	80	–
	400	0.055	80	–
	500	0.045	80	–
	600	0.023	50	4.8
20% V_2O_5–80% TiO_2	110	0.0007	–	–
	300	0.068	40	–
	400	0.070	42	–
	500	0.053	30	10.0
50% V_2O_5–50% TiO_2	110	0.004	1	–
	300	0.181	15	–
	400	0.200	20	–
	500	0.113	15	15.0

* The weight fraction of the catalyst with the ratio V : Ti = 1 : 1.

ratio increasing with an increase in the vanadium content in the binary samples calcined at 300°C and above, as well as a decrease in the lattice parameter c of anatase observed with an increase in the vanadium content (Table 2), can likely indicate the stabilization of vanadium in the anatase structure. The ESR data revealing the presence of the associates of V^{4+} ions in the lattice points of anatase in these samples [72] are in complete agreement with this suggestion. The formation of two species of strongly bound V^{5+} in the distorted octahedral coordination in the vanadium–titanium samples calcined at a low temperature can be explained taking into account that the anatase structure at this calcination temperature is imperfect due to the presence of sulfate ions and water as impurities.

Let us consider possible reasons for the stabilization of vanadium ions in anatase in the preparation of samples as was described above. According to the data on the microstructure of the starting titanium dioxide [78], this can be due to the use of highly dispersed anatase with a disordered structure for preparing catalysts. This structure exhibits microdistortions and vacancies in the cationic sublattice, which can serve as sites for the evolution of a solid-phase process. The defects of the crystal structure of reagents significantly affect the nature of solid-phase interactions, especially in highly dispersed systems possessing a great reaction zone [79]. Apparently, the use of a highly dispersed anatase with a disordered structure and the formation of highly dispersed vanadia crystallites allowed the reaction zone to be considerably expanded and the reactivity of the starting reagents to be enhanced during the solid-phase interaction as compared to well-formed and more coarsely dispersed anatase.

The interaction between anatase and vanadia can occur through the mass transfer of the vanadium ions by both diffusion via known mechanisms [79] and incorporation of the vanadia crystallites into the surface layers of TiO_2 or by the completion of particular regions of the anatase lattice by vanadia crystallites. This completion is probable according to the data on the mathematical simulation of the interaction between vanadia and the surface layers of anatase [50] and to the data [49]. In our opinion, the incorporation of vanadium into the anatase structure and its stabilization in the surface layers of anatase are hardly discernible at the anatase particle size equal to 3–8 nm (4–12 coordination polyhedra).

It follows from the data obtained by the methods used that the highly dispersed anatase crystallites doped by vanadium are stable during thermal treatment at rather high temperatures. The range of their thermal stability decreases with an increase in the vanadium content.

The spontaneous coalescence of highly dispersed anatase crystallites doped by vanadium to large crystals of ~70 nm in size inside the aggregate is accompanied by the formation of coherent boundaries (at a vanadium content ~25 wt %) or the structures of coherent coalescence (at higher vanadium contents) between the V_2O_5 and TiO_2 crystallites with the ratio V : Ti = 1 : 1.

A detailed analysis of the structure of the coherent boundaries formed and coherent coalescence, which was performed in [80], showed that the microstructure is identical at the content 5–50% V_2O_5 and 95–50% TiO_2: the (310) planes of vanadia are joined with the (110) planes of titanium dioxide. The angle between the (001) directions of TiO_2 and V_2O_5 unit cells is equal to 17.4°. The length and number of these boundaries increase with an increase in the vanadium content.

The absence of vanadium from the anatase crystal beyond the boundary region, as well as the formation of

Table 5. Catalytic properties of the vanadia–titania catalysts in the oxidation of β-picoline to nicotinic acid at the 50% conversion of β-picoline

Chemical composition, wt %	T^*, °C	The rate of conversion of β-picoline, $w \times 10^9$, mol m^{-2} s^{-1}	Selectivity for nicotinic acid, %
5% V_2O_5, 95% TiO_2	590	16.0	84
10% V_2O_5, 90% TiO_2	560	16.5	84
15% V_2O_5, 85% TiO_2	500	15.0	83
20% V_2O_5, 80% TiO_2	450	15.0	85
30% V_2O_5, 70% TiO_2	400	16.5	85
50% V_2O_5, 50% TiO_2	300	16.0	84
75% V_2O_5, 25% TiO_2	300	16.0	84
100% V_2O_5	450	4.0	70

* Calcination temperature for the samples of catalysts.

the anatase crystal with a regular structure (Table 2) containing no impurities of sulfate ions and hydroxyl groups (Fig. 5) can indicate that V^{4+} ion associates that replace Ti^{4+} ions at the lattice points of anatase and V^{5+} ions in the distorted octahedral coordination are stabilized in the region of the coherent boundary. A high constant of quadrupole interaction between the V^{5+} ions forming the coherent boundary is evidence of a great gradient of the electrical field on vanadium, and it may be a consequence of the formation of V–O–Ti bonds.

The formation of coherent boundaries and coherent coalescence structures in the vanadia–titania catalysts is responsible for their high activity and selectivity in the oxidation of β-picoline to nicotinic acid. This is likely due to the formation of the V–O–Ti bonds and a change in the state of vanadium cations as compared to that in V_2O_5. This may result in a change in the bond strength of surface oxygen as compared to individual vanadium and titanium oxides [81].

Thus, when vanadia–titania catalysts are prepared by mixing vanadyl oxalate and highly dispersed titanium dioxide with the anatase structure, which is highly imperfect, vanadium is stabilized in anatase during thermal treatment. The structures obtained are reasonably stable in a wide temperature range.

Sintering of the particles of highly dispersed anatase doped by vanadium results in the formation of the coherent boundaries of coalescence between the V_2O_5 and TiO_2 crystallites with the ratio V : Ti = 1. The length and amount of the boundaries increases with an increase in the vanadium content of the samples. The V^{5+} ions in the vicinity of the boundary are in the distorted octahedral coordination.

ACKNOWLEDGMENTS

This work was supported by the Russian Foundation for Basic Research (project nos. 96-03-33087 and 98-03-32323a) and INTAS (grant no. IR-97-0059).

REFERENCES

1. Nikolov, V., Klissurski, D., and Anastasov, A., *Catal. Rev. – Sci. Eng.*, 1991, vol. 33, nos. 3–4, p. 319.
2. Bond, G.C. and Tahir, S.F., *Appl. Catal.*, 1991, vol. 71, no. 1, p. 1.
3. Centi, G., *Appl. Catal.*, 1996, vol. 147, no. 2, p. 267.
4. *Catal. Today*, 1994, vol. 20, no. 1, p. 1.
5. Kantcheva, M.M., Hadjiivanov, K.I., and Klissursri, D.G., *J. Catal.*, 1992, vol. 134, no. 1, p. 299.
6. Wachs, I.E., Salech, R.Y., Chan, S.S., and Chersich, C.C., *Appl. Catal.*, 1985, vol. 15, no. 2, p. 339.
7. Eckert, H. and Wachs, I., *J. Phys. Chem.*, 1989, vol. 93, no. 19, p. 6796.
8. Busca, G., Marchetti, L., Centi, G., and Trifiro, F., *J. Chem. Soc., Faraday Trans. I*, 1985, vol. 81, no. 7, p. 1003.
9. Haber, J., Machey, T., Serwicka, E.M., and Wachs, I.E., *Catal. Lett.*, 1995, vol. 32, nos. 1–2, p. 101.
10. Inumaru, K., Misono, V., and Okuhara, T., *Appl. Catal.*, 1997, vol. 149, no. 1, p. 133.
11. Wachs, I.E. and Weckhuysen, B.M., *Appl. Catal.*, 1997, vol. 157, nos. 1–2, p. 67.
12. Bond, G.C., *Appl. Catal.*, 1997, vol. 157, nos. 1–2, p. 91.
13. Grzybowska-Swierkosz, B., *Appl. Catal.*, 1997, vol. 157, nos. 1–2, p. 263.
14. Salen, R.Y. and Wachs, I.E., *Appl. Catal.*, 1987, vol. 31, no. 1, p. 87.
15. Bond, G.C. and Konig, P., *J. Catal.*, 1982, vol. 77, no. 2, p. 309.
16. Rusieka, M., Grzybowska, B., and Gasior, M., *Appl. Catal.*, 1984, vol. 10, no. 2, p. 101.
17. Dias, C., Portela, M.F., and Bond, G.C., *J. Catal.*, 1995, vol. 157, no. 2, p. 344.
18. Matralis, H.K., Papadopoulou, Ch., Kordulis, Ch., *et al.*, *Appl. Catal.*, 1995, vol. 126, no. 2, p. 365.
19. Andreikov, E.I., *React. Kinet. Catal. Lett.*, 1983, vol. 21, no. 3, p. 351.
20. Cavani, F., Parrinello, F., and Trifiro, F., *J. Mol. Catal.*, 1987, vol. 43, no. 1, p. 117.
21. Santi, V. and Anderson, A., *J. Mol. Catal.*, 1990, vol. 59, no. 2, p. 233.
22. Narayana, K.V., Venugopal, A., Rao, K.S.R., *et al.*, *Appl. Catal.*, 1997, vol. 150, no. 1, p. 269.
23. Hengstum, A.J., Ommet, J.G., Bosch, H., and Geilings, P.J., *Appl. Catal.*, 1983, vol. 8, no. 3, p. 369.
24. Dines, T.J., Rochester, C.H., and Ward, F.M., *J. Chem. Soc., Faraday Trans. I*, 1991, vol. 87, no. 9, p. 1473.
25. Bjorklund, B., Ingemar, O.C.U., Branding, J.G.M., *et al.*, *J. Catal.*, 1989, vol. 119, no. 1, p. 189.

26. Bosch, H. and Janssen, F., *Catal. Today*, 1988, vol. 2, no. 4, p. 369.
27. Sun, Q., Yehng, J.M., Hu, H., *et al.*, *J. Catal.*, 1997, vol. 165, no. 1, p. 91.
28. Bond, G.C., Sarkany, J., and Parfitt, G.D., *J. Catal.*, 1979, vol. 57, no. 3, p. 476.
29. Bond, G.C., Zurita, J.P., Flamerz, S., *et al.*, *Appl. Catal.*, 1986, vol. 22, no. 2, p. 361.
30. Gasior, M., Gasior, I., and Grzybowska, B., *Appl. Catal.*, 1984, vol. 10, no. 2, p. 87.
31. Centi, G., Giamello, E., Pinelli, D., and Trifiro, F., *J. Catal.*, 1991, vol. 130, no. 1, p. 220.
32. Centi, G., Pinelli, D., Trifiro, F., *et al.*, *J. Catal.*, 1991, vol. 130, no. 1, p. 238.
33. Busca, G., Centi, G., Marchetti, L., and Trifiro, F., *Langmuir*, 1986, vol. 2, no. 5, p. 568.
34. Haber, J., Kozlowska, A., and Kozlowski, R., *J. Catal.*, 1986, vol. 102, no. 1, p. 52.
35. Pinaeva, L.G., Lapina, O.B., Mastikhin, V.M., *et al.*, *J. Mol. Catal.*, 1994, vol. 88, no. 1, p. 311.
36. Cartan, F. and Canghlan, C.N., *J. Phys. Chem.*, 1983, vol. 64, no. 25, p. 5176.
37. Hengsum, A.J., Ommen, J.G., Bosch, H., and Gellings, P.J., *Appl. Catal.*, 1983, vol. 7, no. 2, p. 207.
38. Sobalik, Z., Lapina, O.B., Novgorodova, O.N., and Mastikhin, V.M., *Appl. Catal.*, 1990, vol. 63, no. 1, p. 191.
39. Busca, G., *Langmuir*, 1986, vol. 2, no. 5, p. 577.
40. Wachs, I.E., Jehug, J.V., and Hardcastle, F.D., *Solid State Ionics*, 1988, no. 32/33, p. 904.
41. Kozlowski, R., Pettifer, R.F., and Thomas, J.M., *J. Phys. Chem.*, 1983, vol. 87, no. 25, p. 5176.
42. Bond, G.C., Zurita, J.P., and Flamerz, S., *Appl. Catal.*, 1986, vol. 27, no. 2, p. 353.
43. Wachs, I.E., Saleh, R.Y., Chan, S.S., and Chersich, C.C., *J. Catal.*, 1986, vol. 98, no. 1, p. 102.
44. Lapina, O.B., Mastikyin, V.M., Shubin, A.A., Krasilnikov, V.N., and Zamaraev, K.I., *Prog. NMR Spectrosc.*, 1992, vol. 24, p. 457.
45. Went, G.T., Oyama, S.T., and Bell, T., *J. Phys. Chem.*, 1990, vol. 94, no. 10, p. 4240.
46. Rozenboom, F., Mittelmeijer-Hazeleger, M.C., Moulijn, J.A., *et al.*, *J. Phys. Chem.*, 1980, vol. 84, no. 3, p. 278.
47. Deo, G. and Wachs, I.E., *J. Phys. Chem.*, 1991, vol. 95, no. 15, p. 5889.
48. Hausinger, G., Schmelsz, H., and Knozinger, H., *Appl. Catal.*, 1988, vol. 39, nos. 1–2, p. 268.
49. Vejux, A. and Courtine, P., *J. Solid State Chem.*, 1986, vol. 63, no. 1, p. 179.
50. Sayle, D.C., Catlow, R.A., Perrin, M.A., and Nortier, P., *J. Phys. Chem.*, 1996, vol. 100, no. 21, p. 8940.
51. Sanofi, L.R., Walenberg, A., Anderson, S., *et al.*, *J. Catal.*, 1991, vol. 132, no. 1, p. 128.
52. Cristiani, C., Forzatti, P., and Busca, G., *J. Catal.*, 1989, vol. 116, no. 2, p. 586.
53. Al'kaeva, E.M., Andrushkevich, T.V., Zenkovets, G.A., *et al.*, *Stud. Surf. Sci. Catal.*, 1997, p. 939.
54. Popova, G.Ya., Andrushkevich, T.V., and Zenkovets, G.A., *Kinet. Katal.*, 1997, vol. 38, no. 2, p. 285.
55. WO 95/20577, 3.08.95.
56. Bondareva, V.M., Andrushkevich, T.V., and Zenkovets, G.A., Proc. of the 2nd Int. G.K. Boreskov Memorial Conference, Novosibirsk: Boreskov Inst. of Catalysis, 1997, part. 2, p. 164.
57. Tsybulya, S.V., Cherepanova, S.V., and Solov'eva, L.P., *Zh. Strukt. Khim.*, 1996, vol. 37, no. 2, p. 379.
58. Iveronova, V.I. and Revkevich, G.P., *Teoriya rasseyaniya rentgenovskikh luchei* (X-ray Scattering Theory), Moscow: Mos. Gos. Univ., 1978.
59. Chung, F.H., *J. Appl. Crystallogr.*, 1974, vol. 7, p. 579.
60. Shubin, A.A., Lapina, O.B., and Bondareva, V.M., *Chem. Phys. Lett.*, (in press).
61. Malakhov, V.V., Vlasov, A.A., Boldyreva, N.N., and Dovlitova, L.S., *Zavod. Lab.*, 1996, vol. 62, no. 2, p. 1.
62. Malakhov, V.V. and Vlasov, A.A., *Kinet. Katal.*, 1995, vol. 36, no. 4, p. 503.
63. Dobrovol'skii, I.P., *Khimiya i tekhnologiya oksidnykh soedinenii titana* (Chemistry and Chemical Engineering of Titanium Oxides), Sverdlovsk, 1988.
64. Hucknall, D.J. and Cullis, C.F., *J. Thermal Anal.*, 1978, vol. 13, no. 1, p. 15.
65. Altynnikov, A.A., Zenkovets, G.A., and Anufrienko, V.F., *React. Kinet. Catal. Lett.*, 1994, vol. 52, no. 1, p. 59.
66. Nakamoto, K., *Infrared Spectra of Inorganic and Coordination Compounds*, New York: Wiley, 1964.
67. Burgina, E.B., Kustova, G.N., Nikitenko, S.G., *et al.*, *Zh. Strukt. Khim.*, 1996, vol. 37, no. 1, p. 275.
68. Sokolov, D.N., *Gazovaya khromatografiya letuchikh kompleksov metallov* (Gas Chromatography of Volatile Metal Complexes), Moscow: Nauka, 1981, p. 61.
69. Wachs, I.S., *Catal. Today*, 1996, vol. 27. nos. 3–4, p. 437.
70. Busca, G., Ricchiardi, G., Siew Hew Sam., D., and Volta, J.-C., *J. Chem. Soc., Faraday Trans.*, 1994, vol. 90, no. 8, p. 1161.
71. Zenkovets, G.A., Gavrilov, V.Yu., Kryukova, G.N., and Tsybulya, S.V., *Kinet. Katal.*, 1998, vol. 39, no. 1, p. 122.
72. Altynnikov, A.A., Zenkovats, G.A., and Anufrienko, V.F., *React. Kinet. Catal. Lett.*, 1999, vol. 66, no. 1, p. 85.
73. Gavrilov, V.Yu. and Zenkovets, G.A., *Kinet. Katal.*, 1993, vol. 34, no. 2, p. 357.
74. Bond, G.C., *Appl. Catal.*, 1991, vol. 71, no. 1, p. 1.
75. Boldyrev, V.V., Nev'yantsev, I.S., Mikhailov, Yu.I., and Khairetdinov, E.F., *Kinet. Katal.*, 1970, vol. 11, no. 2, p. 367.
76. Vejux, A. and Courtine, P., *J. Solid State Chem.*, 1978, vol. 23, no. 1, p. 93.
77. Maksimovskaya, R.I. and Chumachenko, N.N., *Polyhedron*, 1987, vol. 6, no. 10, p. 1813.
78. Zenkovets, G.A., Tsybulya, S.V., Burgina, E.B., and Kryukova, G.N., *Kinet. Katal.*, 1999, vol. 40, no. 4, p. 623.
79. Tret'yakov, Yu.D., *Tverdofaznye reaktsii* (Solid-State Reactions), Moscow: Khimiya, 1978.
80. Kryukova, G.N., Klenov, D.O., and Zenkovets, G.A., *React. Kinet. Catal. Lett.*, 1997, vol. 60, p. 179.
81. Bondareva, V.M., Andrushkevich, T.V., and Pankratiev, Yu.D., *React. Kinet. Catal. Lett.*, 1997, vol. 61, no. 2, p. 337.